ACS chemical biology

Articles

pubs.acs.org/acschemicalbiology

# ATP Sequestration by a Synthetic ATP-Binding Protein Leads to Novel Phenotypic Changes in *Escherichia coli*

Shaleen B. Korch,[⊥] Joshua M. Stomel,[†,§] Megan A. León,[†] Matt A. Hamada,[⊥] Christine R. Stevenson,[†] Brent W. Simpson,[†] Sunil K. Gujulla,[†] and John C. Chaput*[,†,‡]

[†]Center for Evolutionary Medicine and Informatics, The Biodesign Institute, [‡]Department of Chemistry and Biochemistry, and [§]School of Life Sciences, Arizona State University, Tempe, Arizona 85287-5301, United States

[⊥]Department of Pharmacology, Midwestern University, Glendale, Arizona 85308, United States

**ABSTRACT:** Artificial proteins that bind key metabolites with high affinity and specificity hold great promise as new tools in synthetic biology, but little has been done to create such molecules and examine their effects on living cells. Experiments of this kind have the potential to expand our understanding of cellular systems, as certain phenotypes may be physically realistic but not yet observed in nature. Here, we examine the physiology and morphology of a population of *Escherichia coli* as they respond to a genetically encoded, non-biological ATP-binding protein. Unlike natural ATP-dependent proteins, which transiently bind ATP during metabolic transformations, the synthetic protein DX depletes the concentration of intracellular ATP and ADP by a mechanism of protein-mediated ligand sequestration. The resulting ATP/ADP imbalance leads to an adaptive response in which a large population of bacilli cells transition to a filamentous state with dense lipid structures that segregate the cells into compartmentalized units. A wide range of biochemical and microscopy techniques extensively characterized these novel lipid structures, which we have termed endoliposomes. We show that endoliposomes adopt well-defined box-like structures that span the full width of the cell but exclude the synthetic protein DX. We further show that prolonged DX exposure causes a large fraction of the population to enter a viable-but-non-culturable state that is not easily reversed. Both phenotypes correlate with strong intracellular changes in ATP and ADP concentration. We suggest that artificial proteins, such as DX, could be used to control and regulate specific targets in metabolic pathways.

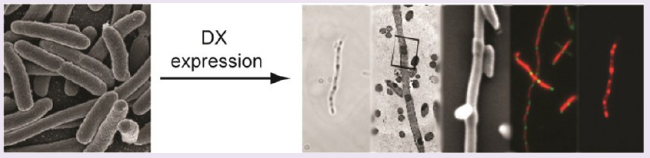


A major goal of synthetic biology is to understand the biology of living systems.[1] Chemists approach this problem by designing abiotic molecules that recapitulate emergent properties of life;[2,3] engineers approach this problem by developing artificial pathways that function inside living systems;[4−6] and geneticists approach this problem by creating living organisms with synthetic genomes.[7,8] We recently described a fourth approach to synthetic biology that involves examining the morphology and physiology of living cells as they respond to an entirely man-made protein from non-biological origin.[9] The motivation for this study was to enhance our understanding of cellular behavior and the decisions that living systems make when forced to interact with synthetic components. We were particularly interested in determining whether cells expressing synthetic parts might reveal something new about biology as living systems have never before been challenged in this way.

Recent advances in protein engineering have made it possible to create artificial proteins that can fold themselves into stable three-dimensional structures.[10] The most notable examples include (i) Top7, an $\alpha/\beta$-protein created by computational design;[11] (ii) protein S-824, a four-helix bundle produced by binary patterning;[12] and (iii) Family B, a class of ATP binding proteins generated by *in vitro* evolution.[13] Of these, only the Family B protein was generated with an intended function, namely, the ability to bind ATP with high affinity and specificity. We have previously optimized the Family B protein for improved folding stability and solubility and solved its three-dimensional structure by NMR and X-ray crystallography.[14−16] This class of synthetic proteins adopts a novel zinc-nucleated $\alpha/\beta$-fold with a unique topology and ATP binding site. DX, a highly evolved member of Family B, has been the subject of numerous biochemical and biophysical studies due to its ability to catalyze the regiospecific hydrolysis ATP to ADP.[17,18]

Given the importance of ATP as the energy source of life and central metabolite in many biological pathways, we wondered how living cells might respond to alterations in their intracellular levels of ATP through a mechanism of protein-mediated ligand sequestration. We reasoned that protein DX provided an ideal opportunity to study this effect and to examine the broader question of how living cells would respond to an encounter with a foreign protein that originated outside of the boundaries that nature defined for cellular proteins.[19] Exploratory studies into the morphology and physiology of *DX*-expressing *E. coli* cells demonstrated that DX transitions *E. coli* into a filamentous state with limited cell division and low metabolic activity.[9] We interpreted this result to mean that DX was disrupting the energy balance of the cell by sequestering

**Received:** March 14, 2012
**Accepted:** November 26, 2012
**Published:** November 26, 2012

   dx.doi.org/10.1021/cb3004786 | *ACS Chem. Biol.* 2013, 8, 451−463

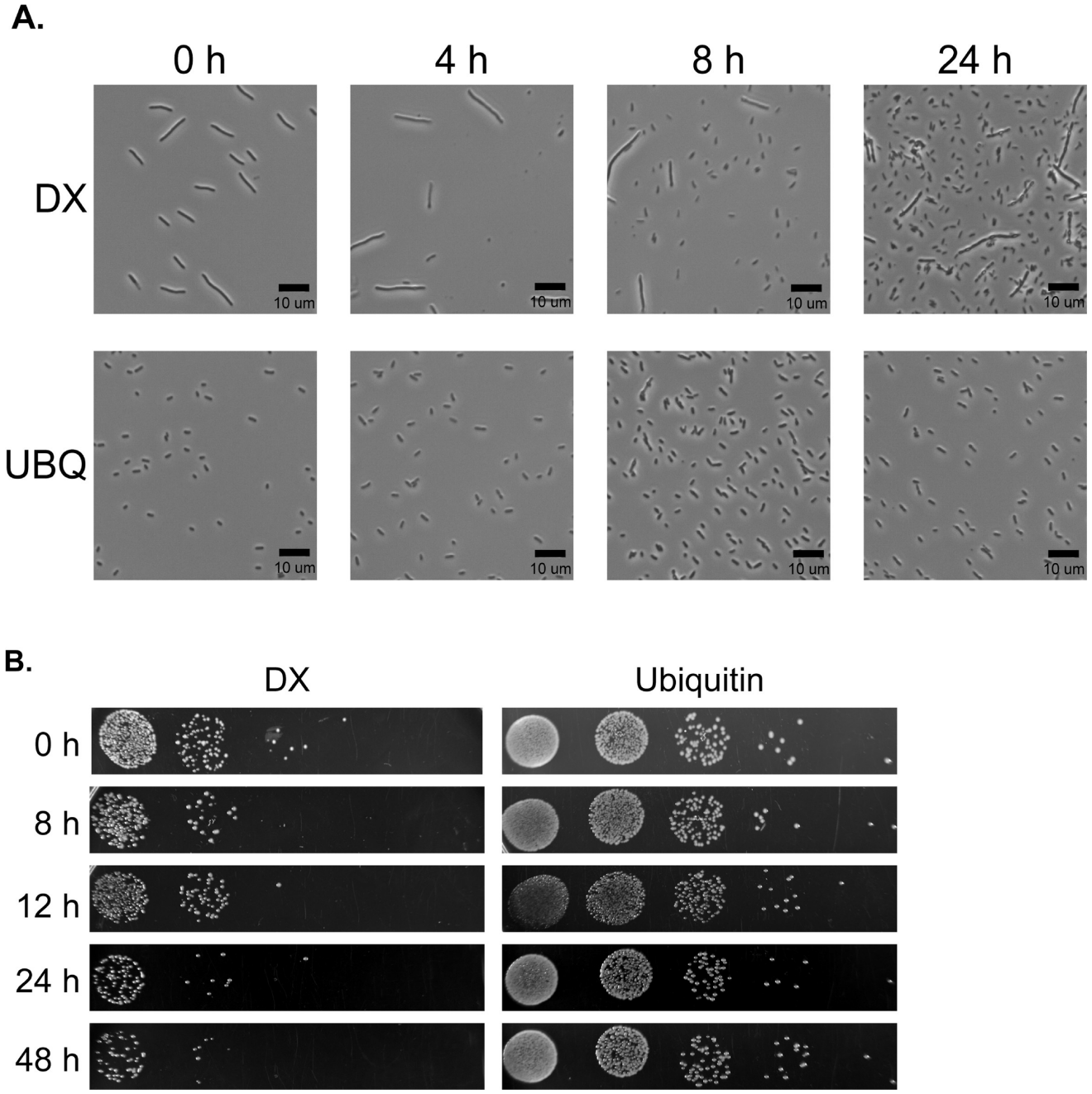


**Figure 1.** Growth inhibition of *E. coli* following expression of a synthetic ATP binding protein. *E. coli* carrying either pBAD18::*DX* or pBAD18::*UBQ* were grown for 8 h at 37 °C in LB media containing arabinose (inducer). Cells were washed, resuspended in fresh LB media without inducer, and grown at 37 °C with aeration. (A) Phase-contrast micrograph images taken between 0 and 24 h of recovery phase growth. Top panels: DX strain. In addition to filamentous cells, a population of bacilli becomes visible after 4 h and grows to dominate the population by 24 h. Images taken between 24 and 48 h of recovery have a similar distribution of filamentous and bacilli cells (data not shown). Bottom panels: Ubiquitin strain. Cells appear as morphologically normal bacilli throughout 24 h of recovery analysis. All images were acquired at 40x magnification. (B) Recovery phase CFU analysis of *E. coli* after *DX* or *ubiquitin* expression. At the times indicated, cells were spotted in 10-fold serial dilutions ($10^{-3}$–$10^{-7}$) onto solid agar plates (without inducer) and incubated at 37 °C for 16 h.

free ATP and ADP molecules present in the cellular milieu. This was a reasonable interpretation since DX was previously shown to bind ATP and ADP with similar low nanomolar affinity, which is far below the intracellular concentration of both molecules in *E. coli*.[16] Whether and to what extent a population of *E. coli* could recover from their exposure to DX are interesting questions that were never addressed in our original study. We envisioned an "exposure phase" in which cells expressing *DX* fall into an ATP/ADP deprived condition that impacts cellular metabolism on a global scale, followed by a "recovery phase" when the cell population would attempt to recuperate following the cessation of *DX* expression. We suspected that complete resuscitation would depend on several factors, including the amount of time the cells were exposed to DX, the extent to which DX has been removed from the cell, and the presence of appropriate biological, chemical, and genetic factors such as resuscitation promoting-factors and quorum sensing molecules.[20,21] Given the growing problem of


dx.doi.org/10.1021/cb3004786 | *ACS Chem. Biol.* 2013, 8, 451–463

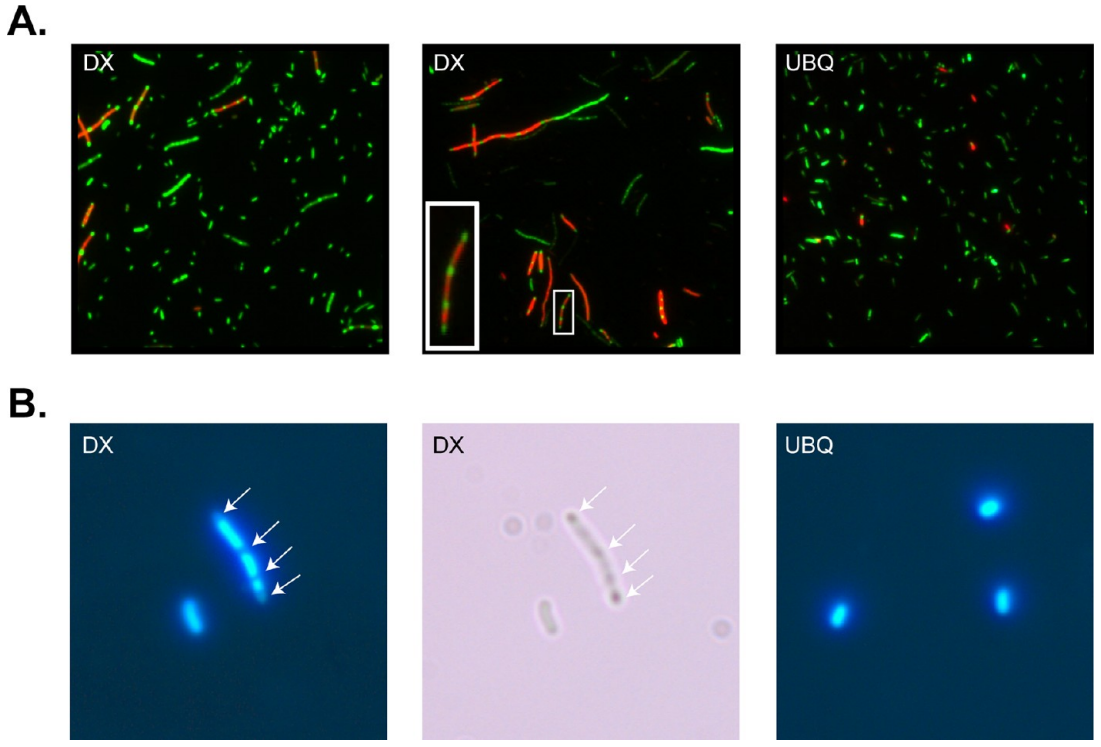


**Figure 2.** Dense intracellular structures and DNA localization in filamentous cells. (A) Fluorescent microscopy images demonstrate the viability of *E. coli* after 24 h of recovery phase growth. Viable cells with intact membranes stain green with SYTO-9. Cells with damaged membranes stain red with propidium iodide. (Left) A representative field of view of cells from the DX strain demonstrates phenotypic variation as a consequence of *DX* expression. Normal bacilli stain green and are viable, while filamentous cells differ considerably in their staining pattern. (Center) A select field of view shows filamentous cells following DX exposure. The inset is a magnified image highlighting the unique staining pattern observed in DX-exposed filamentous *E. coli*. These cells have distinct green foci evenly spaced throughout the filament, indicating nucleic acid compartmentalization. Other cells have staining patterns indicating that one-half of the cell membrane is intact, while the other one-half is compromised. (Right) A random field of view of live cells from the ubiquitin strain. Images were taken at 40x magnification. (B) Fluorescent and phase-contrast micrographs taken at 100x magnification of DAPI-stained *E. coli* after 24 h of recovery phase growth. (Left and center) A representative view of DAPI-stained DX-cells demonstrates that in filamentous cells, DNA localizes outside of the boundaries of the dense intracellular structures. Arrows indicate the position of intracellular structures. (Right) A representative field of view of DAPI-stained cells from the ubiquitin strain.

antibiotic resistance and the unmet need for novel therapeutic agents,[22] we pursued this study with goal of finding new inroads into basic research, biotechnology and molecular medicine. Here we report the effects of *DX* expression and present evidence that ATP/ADP sequestration can trigger a viable-but-non-culturable (VBNC) state in *E. coli*. We further show that entrance into the VBNC state coincides with multiple phenotypic changes, the most prominent of which includes the synthesis of large intracellular lipid structures that we have termed *endoliposomes*, which appear to partition filamentous cells into individual compartments. We postulate that these structures represent a novel adaptation that allows regions of filamentous cells to maintain homeostasis when the membrane of one or more individual compartments becomes compromised.

## RESULTS

***Escherichia coli* Growth Patterns Altered by an Artificial ATP Binding Protein.** *E. coli* strains containing *DX* under the control of an arabinose-inducible promoter (pBAD18::*DX*) were grown under inducing conditions in liquid culture for 8 h. Following expression, arabinose was removed from the media, and the cells were allowed to recover for up to 48 h. In parallel, a control strain carrying human ubiquitin (pBAD18::*UBQ*) was cultured under identical conditions. Ubiquitin was chosen because of its similar size to that of DX and the fact that it is a foreign protein to *E. coli*. Phase-contrast microscopy images collected during the recovery period (Figure 1A) indicate that the population of DX-exposed cells exhibits a strong filamentous phenotype after 8 h of expression (hour 0 of recovery), which is consistent with our previous study on *DX*-expressing cells.[9] However, as recovery proceeds, the population of filamentous cells becomes less abundant as a new population of bacilli becomes visible and eventually dominates the population. The bacilli cells are similar in appearance to *E. coli* cells expressing *ubiquitin*, which appear morphologically normal.

To examine the impact of *DX* expression on cell viability, growth characteristics of both *E. coli* strains were measured over a 48-h recovery period. At times coincident with the microscopic analysis, cells were removed from liquid culture, plated in 10-fold serial dilutions ($10^{-3}$–$10^{-7}$), and CFU production was observed. This analysis revealed a sharp contrast in the number of CFUs observed between the *DX*- and *ubiquitin*-expressing cells. For example, during the recovery period, cells exposed to ubiquitin have an equivalent number of CFUs, while cells exposed to DX show only a limited number of colonies (Figure 1B). This striking observation suggests that (i) DX has a prolonged negative impact on cell growth that extends long after the inducer has been removed from the culture, and (ii) the population of cells that appear morphologically normal by light microscopy might be the


dx.doi.org/10.1021/cb3004786 | *ACS Chem. Biol.* 2013, 8, 451–463

progeny of filamentous cells that underwent cell division but were unable to grow on solid media.

**DX-Exposed Cells Form Novel Intracellular Structures.** The contrasting results between the microscopic analysis and the cell growth assay indicate that DX interferes with cell growth and division. The simplest explanation is that the population of bacilli observed by light microscopy is actually the remnants of lysed cells. We therefore performed a LIVE/DEAD bacterial assay to examine the membrane integrity of *E. coli* cells after *DX* expression.[23] This assay relies on two dyes that intercalate DNA: SYTO-9, which penetrates cell membranes and fluoresces green, and propidium iodide (PI), which can only penetrate permeabilized membranes and fluoresces red. When used together, PI lowers SYTO-9 emission causing bacterial cells with intact membranes to fluoresce green and bacterial cells with compromised membranes to fluoresce red. Micrographs taken after 24 h of recovery indicate that most bacilli observed after *DX* expression fluoresce green, indicating that these cells have intact membranes and are in fact alive (Figure 2A, left panel). This result demonstrates that DX exposure is not lethal to the cell population but instead transits *E. coli* into a state of reduced growth. Consistent with this interpretation is the observation that *E. coli* cells expressing *ubiquitin*, which also fluoresce green, continue to form colonies after arabinose is removed from the media (Figure 2A, right panel).

With respect to the population of filamentous cells observed after *DX* expression, the number of *E. coli* with intact membranes was roughly equivalent to the number of cells with compromised membranes (Figure 2A, left panel). Of the cells that were clearly dead, an unusual staining pattern occurred in which bright green foci were observed at evenly spaced intervals inside the cell (Figure 2A, middle panel inset). More surprising was the observation that some of the filamentous cells segregate such that half of the cell is alive while the other half is dead. To our knowledge, these two phenotypes have not been reported previously in bacteria. One interpretation is that DX-mediated filaments initiate a defense mechanism in which densely packaged material is used to segment the cell into individual compartments. We refer to this model as the "sinking submarine" as cells appear to partition their genetic information into regions that have a higher propensity to stay alive. Just as a naval submarine is divided into a series of watertight compartments, this population of filamentous cells appears to have acquired a mechanism for self-compartmentalization. This phenomenon is reminiscent of the eukaryotic process of autophagocytosis, which is a natural lysosomal degradation pathway essential for cell survival, differentiation, and development.[24] Autophagy has never been observed in bacteria, and since *E. coli* do not contain lysosomes, any such process would presumably follow a distinctly different mechanism. We verified that the compartmentalized regions contain genomic DNA by staining the cells with DAPI, which distinguishes DNA from RNA. As shown in Figure 2B, fluorescent and phase-contrast images taken after 24 h of recovery phase growth indicate that DNA localizes in the compartmentalized regions of filamentous cells.

**Intracellular Structures Are Composed of Densely Packed Lipids That Exclude DX.** We examined the bright green foci observed in the fluorescent images for lipid and DX content. Cells isolated after 24 h of recovery were stained with Nile Red, a dye that is selective for intracellular lipid material.[25] Fluorescent images of filamentous cells reveal ghosting around the membrane with bright red spheroids that superimpose with the intracellular compartments observed in the companion phase-contrast images (Figure 3A). In addition, we also assayed

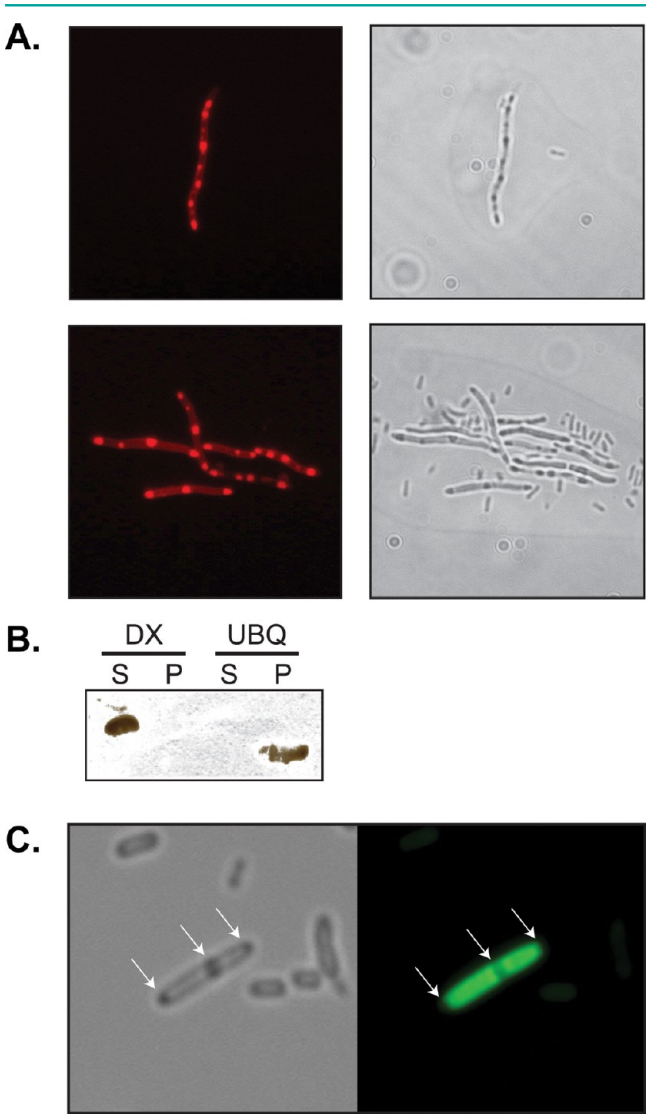


**Figure 3.** Filamentous cells contain evenly spaced lipid compartments that exclude DX. (A) Fluorescent and phase-contrast micrographs (100x magnification) taken of the *E. coli* DX strain after 24 h of recovery phase growth. Cells were stained with Nile Red to detect lipid materials. (B) Western blot analysis of soluble (S) and pellet (P) fractions isolated from *E. coli* after 24 h of recovery phase growth. Mouse anti-FLAG antibody was used to detect both DX and ubiquitin proteins. (C) Fluorescent and phase-contrast micrographs taken of the *E. coli* DX-GFP strain after 24 h of recovery phase growth. Arrows indicate the position of intracellular lipid structures.

the soluble and insoluble fractions of DX- and ubiquitin-exposed cells to determine if the observed intracellular structures contain DX. Western blot analysis indicates that DX remains in the soluble fraction when the cells are lysed and pelleted. The opposite is true for ubiquitin, which resides in the insoluble fraction (Figure 3B). Taken together, these two results demonstrate that the observed intracellular structures are not inclusion bodies, but rather regions of densely packed lipids that exclude DX. We termed these novel intracellular structures "endoliposomes" due to their cellular location and chemical composition. Fluorescence micrographs taken of cells


dx.doi.org/10.1021/cb3004786 | *ACS Chem. Biol.* 2013, 8, 451–463

expressing DX-GFP fusion proteins verified that endoliposomes exclude DX (Figure 3C).

Because our endoliposomes bore a slight resemblance to bacterial endospores observed in certain Gram-positive bacteria, we examined the susceptibility of these structures to standard endospore stains. Using the Shaeffer–Fulton technique,[26] we stained a small population of *E. coli* after 24 h of recovery from DX and ubiquitin. As a positive control, we stained a 3-day-old culture of *Bacillus cereus*. As expected, *B. cereus* gave a mixture of vegetative (pink) and endospore (green) cells (Figure 4). In

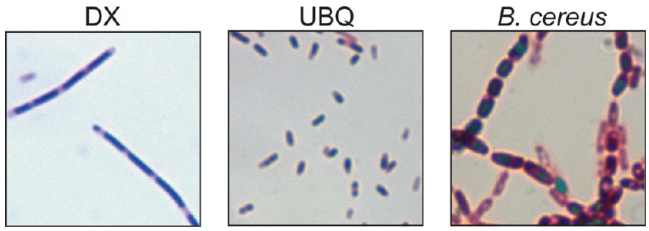


**Figure 4.** DX-induced endoliposomes do not exhibit endospore-like staining properties. Schaeffer–Fulton staining technique was performed on DX or ubiquitin strains following 24 h of recovery growth or to 72-h-old *B. cereus* cells to microscopically assess endospore-like features. (Left) A representative field of view of DX-recovering cells demonstrates that DX exposure does not potentiate the development of endospore-like structures in *E. coli*. Filamentous cells stain purple, consistent with the uptake of both malachite green and safranin, while endoliposomes remain unstained. (Center) A selected field of view of the ubiquitin strain, demonstrating vegetative cells. (Right) A random field of view of 3-day-old *B. cereus* showing both vegetative (pink) cells and endospores (green). All images were taken at 100x magnification.

contrast, DX-induced filaments have unstained regions that coincide with the approximate locations of endoliposomes, suggesting that these structures do not retain the Malachite green stain following decolorization and are therefore not physically or chemically related to endospores. Remaining regions of the filament stains purple, which is consistent with the uptake of both Malachite green and Safranin. Likewise, *E. coli* exposed to ubiquitin also stain purple, although the small size of the bacilli relative to the DX-induced filaments makes this effect more difficult to visualize.

**DX-Induced Filaments Exhibit Limited Cell Division.** Cell growth assays indicate that *DX* expression transits *E. coli* into a viable-but-non-culturable state where the cell population is viable in liquid culture but is incapable of producing colony-forming units on solid media. VBNC is a bacterial condition defined by a state of low metabolic activity that does not support cell division.[27] We examined the potential for DX-induced cells to be resuscitated, as VBNC can, in some instances, be reversed.[27] As a test for VBNC, *E. coli* exposed to DX or ubiquitin were examined for the ability to form microcolonies on solid media containing inducer. After 8 h of induced growth, control cells from the ubiquitin strain form healthy microcolonies that are readily visible by light microscopy, while only a small number of CFUs are observed for the DX-exposed cells (Figure 5A). Furthermore, microcolonies from the DX strain adopt an atypical linear arrangement of cells, while the control strain formed spherical microcolonies typical of *E. coli*.

We examined microcolony formation after 16 h of recovery to determine whether the population of bacilli cells observed in the DX strain are the progeny of filamentous cells. The ubiquitin strain was analyzed in parallel as a positive control for normal microcolony formation. Cells expressing *ubiquitin* undergo rapid cell division and form healthy microcolonies after 4 h at 37 °C, whereas cells from the DX strain lag in growth but eventually form multiple septa along their filaments and divide into daughter cells (Figure 5A). However, cell division in the DX strain appears to arrest after 4 h of growth on solid media as very few microcolonies are observed at later times. This result is consistent with the low CFU count observed in the cell growth assay (Figure 1B) and explains the origin of the live bacilli observed in the microscopic analysis and LIVE/DEAD assays.

**DX Promotes a VBNC State in *E. coli*.** Microcolony analysis confirms that DX filaments are capable of limited cell division. This analysis did not, however, address the physiological state of individual cells once cell division arrests. We speculated that DX-exposed cells enter a persistent state of low metabolic activity that is difficult, if not impossible, to recover from. To test this hypothesis, cells were grown for 8 h with induction and allowed to recover for 16 h in the absence of arabinose. Cells were then plated in serial dilutions and incubated for 24 h at 37 °C (40 h total recovery). Plates without visible CFUs were washed with LB and stained for viability using the LIVE/DEAD assay. This analysis reveals that 89% of the cells in the DX strain were alive, which is consistent with the hypothesis that DX-exposed cells enter a prolonged dormant state (data not shown). Prior to staining, several aliquots were separately inoculated into fresh LB media and incubated at 37 °C with aeration. This attempt at resuscitation failed to produce viable cultures after 48 h (88 h of total recovery) even though live cells were present in the inoculums. In addition, cells expressing *DX* for 24 h exhibited reduced lysis following exposure to ampicillin, a bacteriocidal agent, as compared to cells expressing *ubiquitin* (data not shown). This observation provides further support for reduced division and growth in the DX strain.

We performed a Western blot analysis on samples taken during the expression and recovery phase to determine if DX remained in the cell after arabinose was removed from the culture (Figure 5B). Although protein bands consistent with DX are present throughout the entire recovery period, a considerable drop in protein levels occurs after 24 h of recovery. These results indicate that DX is not easily degraded by cellular proteases and that DX-associated phenotypes are sustained, even when lower amounts of DX are present in the cell. To ensure that this result was not due to leaky expression of *DX* from the pBAD vector, we compared the extent of filamentation observed for the DX and ubiquitin strains after 8 h of uninduced growth and an additional 24 h of simulated recovery. Phase-contrast images revealed a low level of short filamentous cells in both cultures, neither of which contained endoliposomes. Within the population, the frequency of filamentation for the DX strain was not significantly different from that for the ubiquitin strain (0.29% observed in DX strain *vs* 0.13% for ubiquitin strain, statistically similar values, $p > 0.001$). Furthermore, sequence analysis of the *DX* gene from colonies taken after 24 h of recovery did not reveal any mutations in the protein sequence. These data support the hypothesis that *DX* expression in *E. coli* leads to a VBNC state that may be part of a survival mechanism that allows the cell to persist under prolonged conditions of altered intracellular ATP.

**VBNC and Endoliposome Formation Represent ADP/ATP-Dependent Phenotypes.** To determine whether


dx.doi.org/10.1021/cb3004786 | *ACS Chem. Biol.* 2013, 8, 451–463

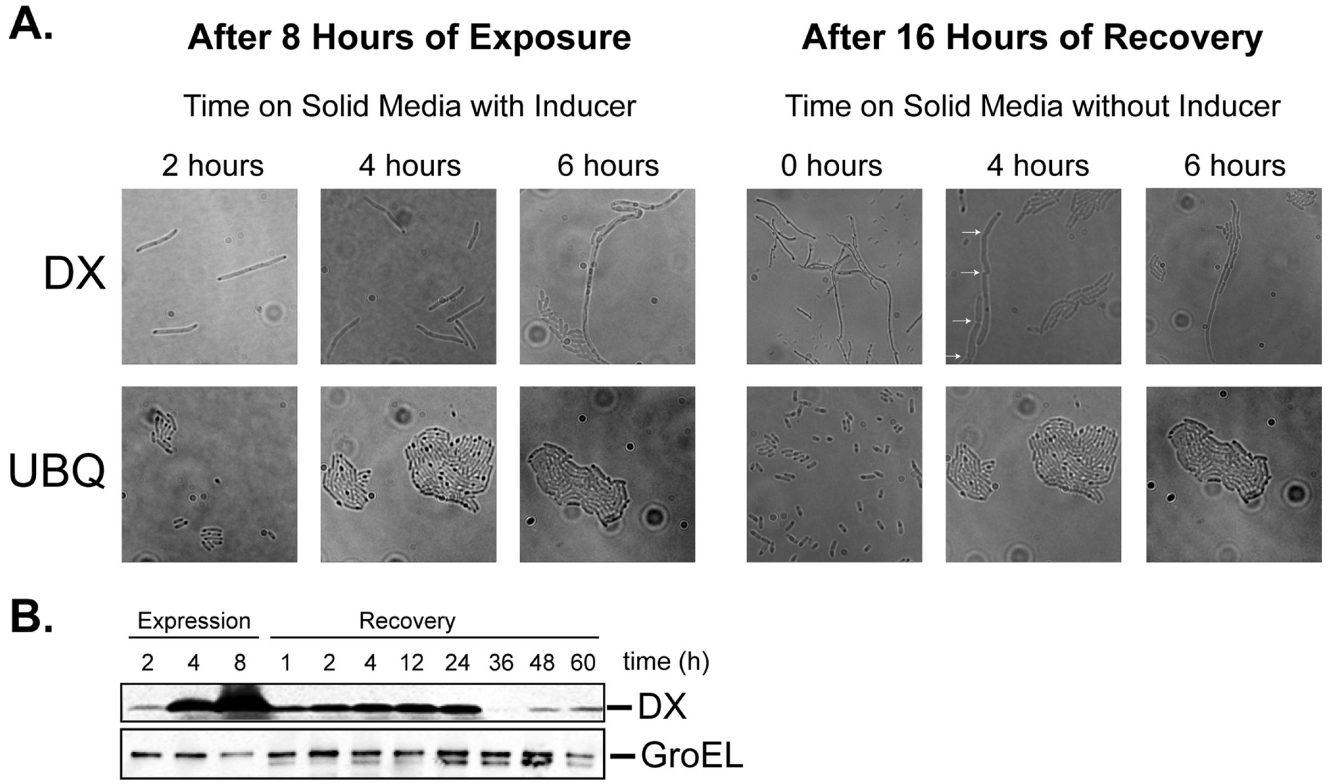


**Figure 5.** Filamentous cells enter a viable-but-non-culturable state after prolonged exposure to DX. (A) *E. coli* transformed with pBAD18::*DX* or pBAD18::*UBQ* were cultured for 8 h in medium containing arabinose to induce *DX* or *UBQ* expression. Aliquots were transferred to slides coated with LB-arabinose to continue *DX* or *UBQ* expression and incubated at 37 °C. Microscopic examination was performed following 2, 4, and 6 h of incubation. To assay cell division during the recovery phase growth, cells expressing *DX* or *UBQ* for 8 h were washed with LB and resuspended in fresh LB without inducer. After 16 h of growth under non-inducing conditions, aliquots were transferred to slides coated with LB and incubated at 37 °C. Microscopic images were collected after 0, 4, and 6 h of incubation. Arrows indicate the locations of individual septa observed in DX-recovering cells. All images were taken at 100x magnification. (B) Western blot analysis of DX during expression and recovery phase growth. Whole cell protein extracts of *E. coli* were assessed at specific times during the expression and recovery phases for the presence of DX and GroEL (loading control).

observed VBNC and endoliposome phenotypes corresponded with changes in intracellular levels of ADP and ATP, we measured ADP and ATP levels in *DX* and *ubiquitin* cultures during active expression and post-expression conditions. Samples were collected at regular intervals during both expression and recovery phase growth (Figure 6). During expression phase growth, ADP and ATP levels in the DX strain approach (in one case go below) the minimum detection limit of the assay, while ATP and ADP levels in the ubiquitin strain increase with time. This observation is consistent with the hypothesis that DX is depleting intracellular ATP and ADP molecules by a mechanism of ligand-binding sequestration. Indeed, solution binding affinity studies reveal that DX binds to ATP and ADP with similar low nanomolar affinity.[17] During recovery phase, ATP levels in both the *DX* and *ubiquitin* cultures return to normal, while ADP levels become elevated until 72 h post-expression (Figure 6). The normalization of ATP and rise in ADP is consistent with the termination of DX synthesis and drop in metabolic drain as the DX strain enters the VBNC state. Under these conditions, it is expected that the cessation of DX synthesis would allow newly synthesized ADP and ATP molecules to remain unbound. However, because the demand for ATP would fall as the cells enter VBNC, ADP levels should rise for a period of time until the system stabilizes. In addition to the reduced demand for ATP, it is also possible that DX, which has weak ATPase activity, could be catalyzing the hydrolysis of some ATP molecules into ADP.[17,18] Taken together, these results are consistent with the prediction that VBNC and endoliposome formation represent two novel ADP/ATP-dependent phenotypes.

**Electron Microscopy Reveals Detailed Intracellular and Extracellular Features.** To gain a better understanding of the size and shape of the observed endoliposome structures, we used transmission electron microscopy to acquire high-resolution images of filamentous *E. coli* after exposure to DX. After 24 h of recovery phase growth, both filamentous and normal bacilli are observed in the electron micrographs taken of DX-exposed cells (Figure 7A). Most *E. coli* filaments contain a high degree of subcellular organization with multiple lipid structures spaced evenly along the length of the cell. Detailed analysis of individual structures reveal that endoliposomes appear as box-like structures with dimensions that are ~1 $\mu$m in length and width. The electron micrographs indicate that endoliposomes do not have a discrete intracellular membrane; however, some endoliposomes are able to amass enough lipid material to force the cell to bulge outward (see below). These structures are not observed in the ubiquitin strain, which contain standard inclusion bodies at a frequency of one per cell (Figure 7B).

We used scanning electron microscopy (SEM) to examine changes to the extracellular surface of *E. coli* after exposure to DX. High-resolution micrographs were collected after 12 and 24 h of recovery phase growth since these times coincided with major phenotypic changes previously observed by light


dx.doi.org/10.1021/cb3004786 | *ACS Chem. Biol.* 2013, 8, 451−463

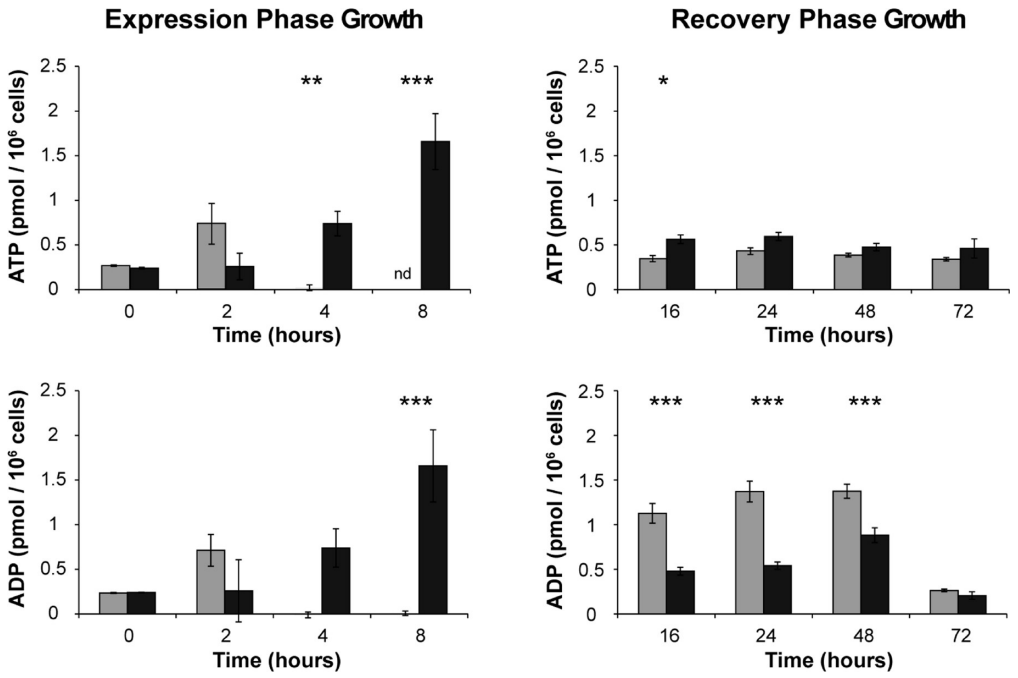


**Figure 6.** Intracellular levels of ATP and ADP in *E. coli* expressing *DX* or *Ubiquitin* during recovery phase. *E. coli* carrying pBAD18, pBAD18::*DX* or pBAD18::*UBQ* were grown for 8 h at 37 °C in LB media containing arabinose (exposure phase). Cells were washed, re-suspended in fresh LB media without inducer, and grown at 37 °C with aeration for an additional 24 hours (recovery phase). At the specified time points, ATP levels were measured for *E. coli* expressing *DX* (grey bars) or *Ubiquitin* (black bars) and the levels of ADP were calculated based on the value of ATP and the ATP:ADP ratio. For statistical analysis, two-way analysis of variance with Bonferroni post tests was used to obtain *P* values for each time point, with the values for *DX* compared to the values obtained for *Ubiquitin*, **, $P < 0.01$; ***, $P < 0.001$.

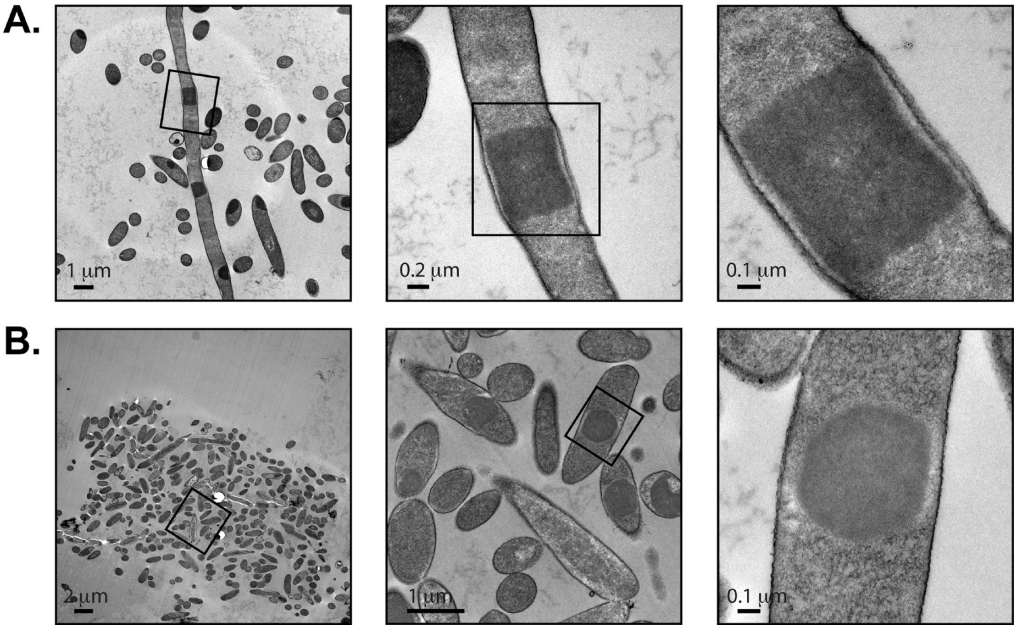


**Figure 7.** High-resolution electron micrographs reveal detailed structural features of DX-induced lipid compartments. (A) Transmission electron microscopy images of filamentous *DX*-expressing *E. coli* taken after 24 h of recovery phase growth. (Left to right) Increasing magnification highlights distinctive intracellular structures observed by light microscopy and fluorescent staining. (B) Transmission electron microscopy images of *ubiquitin*-expressing *E. coli* after 24 h of recovery phase growth. (Left to right) Increasing magnification highlights a typical inclusion body.

microscopy. The resulting SEM images reveal several distinct features of the filamentous and bacilli cells. Immediately apparent was the observation that endoliposomes cause the cell wall to bulge outward, suggesting that these structures have sufficient mass to seal the cell into individual compartments (Figure 8A). Second, the frequency of the endoliposomes increases with time, such that more endoliposomes are visible per unit distance after 24 h than after 12 h (Figure 8A,B). Third, the filamentous cells have regions that differ in cell density and a distinct peapod appearance can be seen after 24 h of recovery with less dense regions occurring in the spaces between endoliposomes. We do not believe that this effect is a


dx.doi.org/10.1021/cb3004786 | *ACS Chem. Biol.* 2013, 8, 451−463

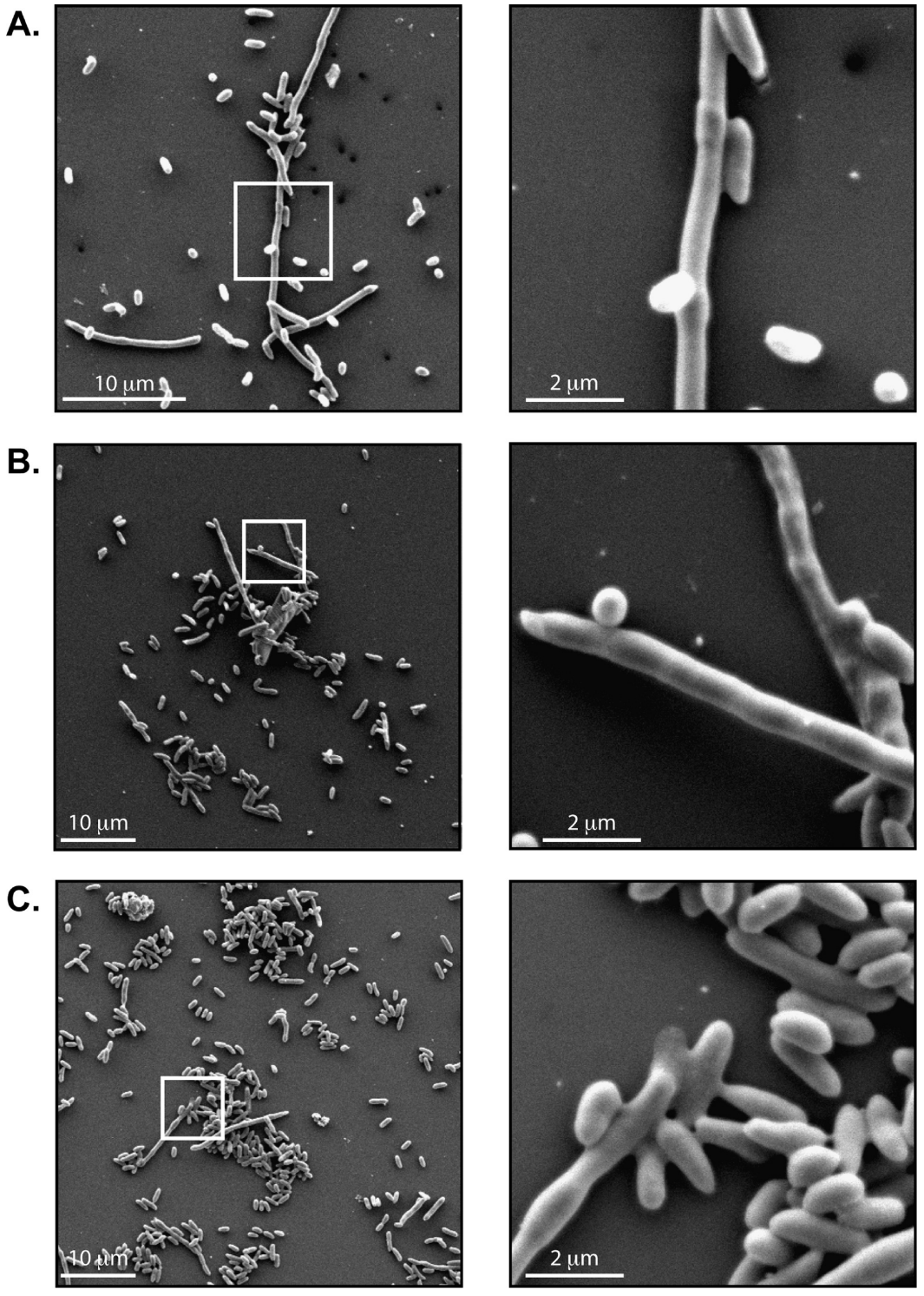


**Figure 8.** High-resolution scanning electron micrographs provide evidence of intracellular and extracellular changes in DX-exposed cells. Scanning electron microscopy images of filamentous *E. coli* DX cells taken after (A) 12 and (B, C) 24 h of recovery phase growth. High magnification images (right panel) of three select fields of view (left panel) reveal several distinct extracellular features of filamentous cells. (A) The cell wall bulges outward at locations where endoliposomes occur inside the cell. (B) Filamentous cells show differences in cytoplasmic density and an increase in the frequency of endoliposomes. (C) Dormant bacilli clump together along filamentous cells. These images confirm many of the properties observed by light and fluorescence microscopy.

result of the staining process as images of filamentous cells collected after 12 h of recovery are uniform in density across the cell. Last, bacilli cells observed after 24 h of recovery appear to be coated with a sticky extracellular layer consistent with polysaccharide formation that causes the cells to adhere to one another (Figure 8C). It is known that defects in the Lon protease, for example, can lead to the production of capsular polysaccharides and filamentous growth in *E. coli*.[28,29] Since Lon is an ATP-dependent protease, it is reasonable that ATP-sequestration by DX prompts *E. coli* to recapitulate the same


dx.doi.org/10.1021/cb3004786 | *ACS Chem. Biol.* 2013, 8, 451−463

phenotypic effects observed by mutant versions of the Lon protease.

## DISCUSSION

Synthetic biology has created a movement in the biological and physical sciences to understand how living systems function.[1] Our approach to this problem has been to explore the biological implications of expressing an artificial protein with a desired function in the environment of a bacterial host organism.[9] This line of research is similar, at least in qualitative terms, to previous studies in which chemists have combined organic chemistry and molecular biology to build unnatural nucleic acid systems that function in living cells.[30] We have focused our studies on DX, an *in vitro* evolved protein that folds into a structure that binds ATP and ADP with high affinity and specificity.[16] We were driven by the question of whether biological systems exposed to a synthetic protein might reveal something new about biology as living systems have never before been challenged in this way. In the context of synthetic biology, experiments of this type have the potential to inform us about the adaptive capabilities of cellular organisms and their ability to sense and respond to changes in intracellular conditions. Problems in adaptive evolution can be quite challenging to solve because it is often difficult to establish the causal relationship between an observed phenotype at the organismal-level and its underlying molecular mechanism. This complexity is due, in part, to such genetic properties as epistasis and pleiotropy, which occur when the effects of one gene are modified by other genes or when a single gene exhibits multiple phenotypic traits, respectively.[31,32]

Previously, we have shown that a population of *E. coli* exposed to DX experience reduced reproductive competency after just 3 h of growth.[9] Changes in cell growth were contemporaneous with the first detection of DX inside the cell and the transition to a filamentous phenotype. Detailed microarray analysis showed a downward trend in biosynthetic pathways responsible for the synthesis of important cell building blocks (*e.g.*, amino acids, nucleotides, and disaccharides) and an upward trend in genes related to cell mobility, sulfur metabolism, and ATP synthesis by salvage pathways.[9] Interestingly, no significant change was observed in SOS response genes, which is the primary mechanism of filamentation in *E. coli*.[33] However, repression was observed for many genes induced by RpoS, suggesting that filamentous growth could be due to an alternative stress response, such as the stringent response pathway promoted by RelA and SpoT.[34] Alternatively, it is also possible that DX disrupts cell division by interfering with certain ATP-dependent proteins such as MinD and FtsA that help position the division septum at the cell equator.[35,36] On the basis of these observations, we proposed an initial model where ATP sequestration by DX leads to an energy-depleted state that limits cell division and impacts cell physiology on a global scale.

Whether and to what extent a population of *E. coli* could recover from the stress of altered intracellular ATP was never addressed in our original study. One might expect *a priori* that following cessation of *DX* expression, ATP levels would rise and the cell would return to a normal physiological state with a healthy metabolism. However, it is also possible that the severe stress of ATP depletion would cause the cell to become reprogrammed in such a way that it is no longer able to revert back to the same physiological state observed in untreated cells. This latter scenario is particularly interesting as cellular reprogramming is an important aspect of synthetic biology that remains poorly understood.[37] Intrigued by the possibility of discovering novel adaptations in *E. coli*, we created an exposure phase in which a population of cells actively expressed *DX* for a defined period of time (8 h), followed by a much longer recovery phase (up to 48 h) in which cells were allowed to recuperate following removal of the inducer.

Three common methods have been used to deplete ATP in *E. coli* and *Salmonella typhimurium*. These include (i) treatment with arsenate, (ii) treatment with $\alpha$-methylglucoside and sodium azide, and (iii) the use of *hisF* mutants starved of histidine.[38] These treatments result in ATP depletion and the inability for ATP repletion without the addition of exogenous chemicals (*i.e.*, adenine, phosphate). DX also creates an ATP-depleted environment, but by an altogether different mechanism that does not eliminate intracellular ATP. Rather, DX sequesters ATP, making it unavailable for ATP-dependent cellular processes. Traditionally, experiments analyzing ATP depletion by the aforementioned methods have focused on bacterial chemotaxis and deciphering biosynthetic and metabolic pathways. In contrast, our analysis of DX focused on *E. coli*'s adaptive response to perceived ATP depletion and in doing so has revealed novel bacterial phenotypes that, to our knowledge, have not been observed in bacteria.

By studying *E. coli* during the recovery phase, we were able to identify several dramatic changes in cell physiology and morphology that were specific to the DX-exposed cell population. The first occurs after ~12 h of recovery phase growth when filamentous *E. coli* form large intracellular structures at regular intervals. These structures are readily visible by phase-contrast microscopy and fluorescence imaging with contrast agents like Nile Red and propidium iodide indicate a lipid composition. While lipid droplets are a known phenotype in bacteria,[39] to our knowledge lipid structures of this size have not been witnessed previously in bacteria. For this reason, we have given these structures the name endoliposome to describe their cellular location and chemical composition. High-resolution TEM and SEM micrographs indicate that endoliposomes adopt well-defined box-like structures that span the full width of the cell and lead to bulges in the cell membrane that gives a distinct peapod-like appearance. Western blot analysis and GFP tagging indicate that endoliposomes exclude DX and are therefore not a new type of inclusion body.

One of the most intriguing aspects of endoliposomes is their ability to partition *E. coli* filaments into individual compartments. We first observed this phenomenon in fluorescent micrographs that were intended to determine the relative proportion of live-dead cells in a population of *E. coli* that were exposed to DX. In addition to showing that the progeny of DX-exposed cells were viable in liquid culture, these micrographs revealed an unexpected property of filamentous *E. coli* in which many of the DX-exposed filaments contained regions that stain separately with SYTO-9 and propidium iodide. This unanticipated result implied that within the boundaries of a single filamentous cell are regions where the membrane is intact and other regions where the membrane is compromised. We reasoned that the only way that this could occur was if the endoliposomes were sealing the filament into individual compartments. This prediction was subsequently verified by electron micrographs taken after 24 h of recovery, which showed that endoliposomes amass sufficient lipid material to partition cell into individual sections.


dx.doi.org/10.1021/cb3004786 | *ACS Chem. Biol.* 2013, 8, 451−463

On the basis of these observations, we propose a model called the "sinking submarine" where filamentous *E. coli* utilize endoliposomes to partition their nutrients into regions that have a higher propensity to stay alive. Our model is an analogy to naval submarines, which use watertight doors as a mechanism for limiting damaged areas to small sections of the ship. This analogy is somewhat reminiscent of the eukaryotic process of autophagocytosis, which is a natural degradative pathway that allows for survival, differentiation, and development.[24] Since *E. coli* do not contain the necessary genes for autophagy, any such process would presumably follow a very different mechanism. One could imagine a relatively simple mechanism in which lipid structures assemble and seal off portions of the cell in response to an immanent threat. Such a scenario would require the rapid orchestration of numerous cellular decisions. This hypothetical response is not entirely unprecedented and direct experimental evidence exists in other organisms found in nature. The hyphae of filamentous fungi, for example, produce dense inorganic particles that plug the pores of perforated septa.[40] While these structures allow for the regulated passage of ribosomes, mitochondria, and nuclei between cells, they also restrict the effects of cellular damage to individual cells.[41] The fact that DX-exposed cells could develop a similar adaptive response provides additional evidence to the emerging view that bacteria are much more sophisticated than previously thought.[42]

The second major change in cell physiology and morphology that occurs as a result of DX-exposure is the ability of *E. coli* to enter a prolonged viable-but-non-culturable state. VBNC is a protective mechanism that many marine, plant and human pathogens use to avoid death.[21,27,43] In certain infectious agents such as enterohemorrhagic *E. coli*, *Helicobacter pylori*, *Pseudomonas aeruginosa* and *Listeria monocytogenes*, VBNC is a major health threat as cell dormancy can provide protection against antibiotics that are used to combat these microorganisms. Consequently, the underlying mechanisms responsible for the entrance, maintenance, and exit of the VBNC state are poorly understood,[44] and cases have been reported where pathogens have emerged after prolonged periods of cell dormancy.[21] Unraveling the mysteries of VBNC is an important goal in biomedical research, as new techniques are urgently needed to detect and fight infectious agents that enter this protective state. The observation that *DX* expression, presumably via ATP/ADP sequestration, can trigger a VBNC state in *E. coli* is interesting on multiple levels. First, it provides a new paradigm for conducting VBNC studies in a model nonpathogenic organism that does not require significant biosafety precautions. In this sense, DX becomes a genetically controlled synthetic element that can be used to rapidly induce VBNC in a population of bacteria. We suspect that the mechanism of action of this genetic tool is significantly different than exogenous small molecule agents, like antibiotics, or environmental stresses that are currently used to establish VBNC in pathogentic organisms.[27] Second, the inability of VBNC cells to recover following the cessation of *DX* expression suggests that ATP deprivation is a possible avenue for new antibiotic development. Given the importance of ATP as a critical energy source, it is difficult to see how any organism, prokaryotic or eukaryotic, could overcome or undergo resistance to severe ATP suppression. One could imagine, for example, using engineered phage to deliver the *DX* gene to pathogenic agents as an alternative to traditional antibiotics. Similar synthetic biology approaches have been used to attack various antibiotic resistance mechanisms in bacteria.[45,46]

In summary, we examined the biology of living cells as they respond to an artificial ATP-binding protein expressed in a population of *E. coli*. We present evidence that DX, a genetically controlled synthetic element, induces a viable-but-non-culturable state in *E. coli* that could not be reversed. We show that onset of the VBNC state coincides with major alterations in intracellular levels of ADP and ATP and the synthesis of dense lipid structures called endoliposomes that partition filamentous cells into individual compartments. While the precise molecular mechanism of endoliposome formation is not yet known, we speculate that these structures function to protect the cell and its genetic contents under severe adverse conditions. These findings highlight the importance of synthetic non-biological proteins as molecular tools for advancing our understanding of biology by targeting specific molecules in complex metabolic pathways.

## METHODS

**Media and Chemicals.** Bacteria were grown on Luria–Bertani (LB) agar plates or in LB broth. Antibiotics (US Biological) were used at the following concentrations: ampicillin (amp), 100 $\mu$g mL$^{-1}$; chloramphenicol (cam) 50 $\mu$g mL$^{-1}$; kanamycin (kan) 50 $\mu$g mL$^{-1}$.

**Strains and Plasmids.** All experiments performed in this study used *E. coli* TOP10 cells (Invitrogen). *DX* and *ubiquitin* were expressed from pBAD plasmids pBAD18::*DX* and pBAD18::*UBQ*, respectively, by adding 0.1% arabinose to the culture.[9] *DX* along with a linker (GSAGSAAGSGEF) and eGFP was constructed by PCR using Accuprime Taq (Invitrogen) to incorporate *Sac* I and *Hind* III restriction sites.[47] The PCR product was cloned into pBAD18 and confirmed by DNA sequencing.

**Recovery Phase Growth Analysis.** *E. coli* transformed with pBAD18::*DX* or pBAD18::*UBQ* were grown at 37 °C with aeration for 14–16 h in LB-amp media, diluted, and resuspended in fresh LB-amp media containing arabinose to induce gene expression. Cells were grown under inducing conditions for 8 h (exposure phase), washed twice with fresh LB, resuspended without dilution in fresh LB-amp, and grown at 37 °C with aeration for up to 48 h (recovery phase).

**Cell Morphology by Phase-Contrast Imaging.** Aliquots (1 mL) were removed at 0, 4, 8, 24, and 48 h into recovery. A small portion was diluted in sterile PBS and spotted as a series of five 10-fold serial dilutions onto LB-amp agar plates. The plates were incubated for 16 h at 37 °C and imaged using a Bio-Rad Gel Doc XR+ system. Cell morphology was accessed by centrifuging the remaining aliquot for 5 min at 5,000 rpm. The supernatant was removed, and the pellet was resuspended and fixed for 20 min in a 4:1 solution (0.5 mL) of PBS/glutaraldehyde (8%). To prepare cells for viewing, the PBS/glutaraldehyde solution was removed, and the cells were resuspended in 0.5 mL PBS. The cell concentration was further adjusted with PBS as needed for optimal viewing, and cells were visualized using a Fisher Scientific Micromaster microscope at 40x magnification. This experiment was performed in triplicate.

**Cell Filamentation of Uninduced Samples.** Phase-contrast images were collected as described above for DX and ubiquitin strains with the exception that cells were grown in the absence of inducer for 8 h followed by simulated recovery for an additional 24 h. Multiple images were collected, and cells were manually counted and scored as normal or filamentous (DX, $n$ = 5245; Ubq, $n$ = 3554).

**Live/Dead Fluorescence Imaging.** A LIVE/DEAD BacLight bacterial viability kit (Invitrogen) was used to assess the integrity of *E. coli* membranes during recovery. After 8, 12, and 24 h of recovery, 1 mL aliquots were removed from the liquid culture and processed immediately. Samples were washed twice with 0.85% NaCl and resuspended in 1 mL of 0.85% NaCl. Then 1.5 $\mu$L of a 1:1 solution of SYTO-9 and propidium iodide were added to 500 $\mu$L of suspended cells, and the mixture was incubated in the dark for 10 min at RT.


dx.doi.org/10.1021/cb3004786 | *ACS Chem. Biol.* 2013, 8, 451–463

Cells were then imaged at 40x magnification with a Zeiss Axioskop 40 fluorescent microscope. This experiment was performed in triplicate.

**DAPI Fluorescence Imaging.** After 24 h of recovery, 1 mL aliquots of *E. coli* cells carrying pBAD18::*DX* or pBAD18::*UBQ* were removed from the culture, stained with DAPI, and prepared for microscopy as described by Schmidt.[48] Cells were imaged at 100x magnification with a Zeiss Axioskop 40 fluorescent microscope. This experiment was performed in triplicate.

**Phase-Contrast and Fluorescence Imaging of GFP-Tagged DX.** Phase-contrast and fluorescence images were collected after 16 h of recovery phase growth in MG1655 *E. coli* strain. Cells were pelleted by centrifugation at 5000 × *g* for 5 min, and the cell pellet was resuspended in 0.5% paraformaldehyde in phosphate buffered saline (PBS) and incubated for 30 min at RT for fixation. Fixed cells were washed with PBS for at least five times and resuspended in PBS. Cells were stored at 4 °C until microscope images were collected. A suspension of fixed cell (~5 μL) was deposited onto poly L-lysine coated coverslips (BD biosciences, USA) and incubated for 5 min at RT before inverting on a glass slide. Phase-contrast and GFP fluorescence images were collected using a Zeiss (Axioskop 40) Fluorescent microscope at 100X magnification.

**Nile Red Fluorescence Imaging.** After 24 h of recovery, 1 mL aliquots were removed from the culture and centrifuged for 5 min at 5,000 rpm. The pellet was resuspended in 150 mM NaCl with 0.1 μg/mL Nile Red dye and incubated for 10 min at 24 °C. The cells were then washed twice with PBS and resuspended in PBS. Cells were visualized at 100x magnification. Phase-contrast and fluorescence microscopy were performed with a Nikon Optiphot 2 microscope and imaged with a Pixera 600CL CCD digital camera. This experiment was performed in triplicate.

**Schaeffer–Fulton Staining for Endospores.** *E. coli* cells carrying pBAD18::*DX* or pBAD18::*UBQ* were grown as described for recovery phase growth analysis. As a positive control for endospore formation, spores of *B. cereus* were inoculated in fresh LB media and grown at 37 °C with aeration for 72 h. This time point was chosen to illustrate both vegetative and spore cells of *B. cereus*. Following 24 h of recovery (DX) or three days of growth (*B. cereus*), heat fixed slides were individually prepared and stained with a Schaeffer and Fulton Spore Stain Kit (Sigma) according to the manufacturer's instructions. The slides were imaged under oil immersion at 100x magnification with a Zeiss Axioskop 40 fluorescent microscope. This experiment was performed in duplicate.

**Microcolony Analysis.** Slides were prepared by dipping into ethanol for sterilization followed by dipping into liquid LB-agar at 55 °C. Slides were immediately placed on a level surface to allow the agar to solidify. The bottom of the slide was wiped off to remove agar and then cleaned with ethanol. Culture aliquots (from exposure and recovery phase) were diluted, and 3 μL was spread onto the surface of the prewarmed agar slide using a pipet tip. A 24 mm × 40 mm coverslip was placed onto the agar and gently pressed into place. Slides were incubated in a humidity chamber at 37 °C and removed at the indicated times for photography. Phase-contrast microscopy was performed with a Nikon Optiphot 2 microscope and photographed with a Pixera 600CL CCD digital camera. This experiment was performed in duplicate.

To assess the viability of cells capable of forming a microcolony but unable to form a CFU, 100 μL of diluted culture ($10^{-3}$–$10^{-8}$) in the recovery phase (8 h expression and 16 h recovery) was plated on LB-amp agar and incubated at 37 °C for 24 h. Plates without visible CFUs were washed with 2 mL of prewarmed LB and centrifuged, and cells were resuspended in 400 μL of prewarmed LB media. Then 300 μL of cells were stained with SYTO-9 and propidium iodide as described for LIVE/DEAD fluorescent staining and observed microscopically for viability. To assess the ability of cells to resume growth, the remaining 100 μL of cells were inoculated into 5 mL prewarmed LB-amp and grown with aeration at 37 °C. Following 24 and 48 h of incubation, cultures were analyzed for turbidity. This experiment was performed in duplicate.

**Western Blot Analysis.** Sample aliquots were removed after 2, 4, and 8 h of expression and 1, 2, 4, 12, 24, 36, 48, and 60 h of recovery, and cells were pelleted by centrifugation, resuspended in lysis buffer (PBS with 0.2 mg/mL lysozyme, 1 mM DTT, PMSF, and RQ1 DNase), and incubated for 20 min at 37 °C. The protein concentration of each cell lysate was determined using a Bradford assay, and equal protein amounts were mixed (1:1) with Laemmli Sample Buffer (Bio-Rad) supplemented with 5% β-mercaptoethanol and heated at 100 °C for 5 min. Protein samples were resolved in a 4–12% SDS-PAGE gel (Invitrogen) and then transferred onto a nitrocellulose membrane. Membranes were blocked with Odyssey Blocking Buffer (Li-Cor) and incubated with mouse anti-FLAG antibody (1:1,000, Cell Signaling Technology) and rabbit anti-GroEL antibody (1:50,000, Sigma, loading control) overnight at 4 °C. Signal was developed using goat anti-rabbit and goat anti-mouse antibodies conjugated with a fluorescent tag (1:15,000, Li-Cor) and imaged using a Li-Cor Odyssey CLx. This experiment was performed in duplicate.

**DX Localization Analysis.** To determine the intracellular location of the DX protein, Western blot analysis was performed as described above with the following modifications. Samples of *E. coli* carrying either pBAD18::*DX* or pBAD18::*UBQ* were assayed 24 h into the recovery phase. The cells were sonicated at 4 °C and pelleted by centrifugation at 16,000 rpm in a Beckman-Coulter Avanti J-E centrifuge. The soluble fraction was removed, and the pellets were washed in wash buffer (PBS with 1 mM DTT and 1% Triton X-100) and resuspended in PBS with 1 mM DTT. Soluble and pellet fractions were resolved on a 4–14% SDS-PAGE gel, transferred to a nitrocellulose membrane, and processed as described. This experiment was performed in duplicate.

**Determination of ADP and ATP levels.** To assess the levels of ADP and ATP, cells overexpressing *DX*, *ubiquitin*, or the empty vector were grown as described for recovery phase analysis. At the specified time points during the expression and recovery phases of growth, 250 μL of culture was removed and lysed using 1% trichloroacetic acid (TCA) as previously described.[49] Following TCA treatment, 0.02 M NaOH was added to stop cell lysis, and 250 μL of 6X Tris acetate buffer was added to neutralize the pH of the lysate. Samples were centrifuged and the protein concentration of each cell lysate was determined using a Bradford assay. The ratio of ATP to ADP was then determined for equal protein amounts from each cell lysate using the ApoSENSOR ADP/ATP Ratio Assay Kit according the manufacturer's instructions (BioVision Inc.). For each sample, cellular levels of ATP were quantified using the Staybrite ATP assay kit (BioVision Inc.) and standards of known ATP concentrations, according to the manufacturer's instructions. Cellular ADP levels were calculated based on the value of ATP and the ATP to ADP ratio. Bioluminescence was detected using a Biotek Synergy 2 luminometer.

**Transmission Electron Microscopy (TEM).** After 24 h of recovery, *E. coli* cultures were fixed in 2% gluteraldehyde buffered in PBS (100 mM $Na_3PO_4$, pH 7.0 and 100 mM NaCl) for 2 h at RT. Cells were washed twice with PBS, resuspended in PBS, and embedded in 1% agarose. The agarose-embedded cell pellets were washed twice with PBS and fixed in 1% osmium tetroxide (buffered in PBS) for 2 h at 24 °C. Pellets were washed twice in $dH_2O$ and suspended in $dH_2O$ overnight at 4 °C. The following day, pellets were washed twice in $dH_2O$ and incubated in 1% uranyl acetate for 2 h at RT, followed by four washes in $dH_2O$. The pellets were dehydrated in an ascending series (20% increments) of 10 min acetone washes with three final wash steps in 100% acetone and infiltrated with Spurr's epoxy resin sequentially (25% increments) with three final washes in 100% resin. Cells were embedded in fresh resin and polymerized for 24 h at 60 °C. Thin sections (70 nm) were cut using an Ultracut-R microtome (Leica Microsystems, Vienna, Austria). Sections were captured on Formvar-coated, 300-mesh copper grids, poststained for 5 min with 1% uranyl acetate and 3 min with Sato's lead citrate. Sections were imaged either with a Philips CM12 TEM or with a JEOL 1200 EX TEM, both operated at 80 kV. Images were generated with either a Gatan 791 CCD camera (CM12) or a Scientific Instruments and Applications L3C model camera (JEOL). This experiment was performed in duplicate.

**Scanning Electron Microscopy.** Cells were removed after 0, 8, 12, and 24 h of recovery and fixed in 2% gluteralehyde buffered in

Dulbecco's PBS and washed three times in PBS. Cells were allowed to adhere to a 0.1% poly-L-lysine coated coverglass slide for 5 min, and then slides were washed with PBS. The immobilized cells were then fixed in 2% osmium tetroxide for 30 min at RT, washed three times with water, and dehydrated in 5 min washes in a sequential acetone series (20%, 40%, 60%, 80%, 3 × 100%). The samples were critical point dried in a Balzers 020 critical point dryer, attached to aluminum mounting stubs, sputter coated with with Au–Pd in Technics Hummer II unit, and imaged on an FEI XL-30 ESEM. This experiment was performed in duplicate.

## AUTHOR INFORMATION

### Corresponding Author

*E-mail: john.chaput@asu.edu.

### Notes

The authors declare no competing financial interest.

## ACKNOWLEDGMENTS

We would like to thank J. Clark-Curtiss for helpful comments and discussions on this manuscript. We would also like to thank the W. M. Keck Bioimaging Laboratory and The Electron Microscopy Laboratory in the School of Life Sciences Bioimaging Facility at ASU. This work is supported by grants from the National Science Foundation (MCB0821032) and the US Army Research Laboratory (W911NF-10-1-0298) to J.C.

## REFERENCES

(1) Benner, S. A., and Sismour, A. M. (2005) Synthetic biology. *Nat. Rev. Genet. 6*, 533–543.

(2) Mansy, S. S., Schrum, J. P., Krishnamurthy, M., Tobe, S., Treco, D. A., and Szostak, J. W. (2008) Template-directed synthesis of a genetic polymer in a model protocell. *Nature 454*, 122–125.

(3) Szostak, J. W., Bartel, D. P., and Luisi, P. L. (2001) Synthesizing life. *Nature 409*, 387–390.

(4) Leonard, E., Nielsen, D., Solomon, K., and Prather, K. (2008) Engineering microbes with synthetic biology frameworks. *Trends Biotechnol. 26*, 674–681.

(5) Pryciak, P. M. (2009) Designing new cellular signaling pathways. *Chem. Biol. 16*, 249–254.

(6) Khalil, A. S., and Collins, J. J. (2010) Synthetic biology: applications come of age. *Nat. Rev. Genet. 11*, 367–379.

(7) Lartigue, C., Glass, J. I., Alperovich, N., Pieper, R., Parmar, P. P., Hutchison, C. A., Smith, H. O., and Venter, J. C. (2007) Genome transplantation in bacteria: changing one species to another. *Science 317*, 632–638.

(8) Gibson, D. G., Glass, J. I., Lartigue, C., Noskov, V. N., Chuang, R.-Y., Algire, M. A., Benders, G. A., Montague, M. G., Ma, L., Moodie, M. M., Merryman, C., Vashee, S., Krishnakumar, R., Assad-Garcia, N., Andrews-Pfannkoch, C., Denisova, E. A., Young, L., Qi, Z.-Q., Segall-Shapiro, T. H., Calvey, C. H., Parmar, P. P., III, C. A. H., Smith, H. O., and Venter, J. C. (2010) Creation of a bacterial cell controlled by a chemically synthesized genome. *Science 329*, 52–56.

(9) Stomel, J. M., Wilson, J. W., Leon, M. A., Stafford, P., and Chaput, J. C. (2009) A man-made ATP-binding protein evolved independent of nature causes abnormal growth in bacterial cells. *PLoS ONE 4*, e7385.

(10) Watkins, J. L., and Chaput, J. C. (2008) Searching combinatorial libraries for native proteins with novel folds. *ChemBioChem 9*, 1361–1363.

(11) Kuhlman, B., Dantas, G., Ireton, G. C., Varani, G., Stoddard, B. L., and Baker, D. (2003) Design of a novel globular protein fold with atomic-level accuracy. *Science 302*, 1364–1368.

(12) Wei, Y. N., Kim, S., Fela, D., Baum, J., and Hecht, M. H. (2003) Solution structure of a de novo protein from a designed combinatorial library. *Proc. Natl. Acad. Sci. U.S.A. 100*, 13270–13273.

(13) Keefe, A. D., and Szostak, J. W. (2001) Functional proteins from a random-sequence library. *Nature 410*, 715–718.

(14) Chaput, J. C., and Szostak, J. W. (2004) Evolutionary optimization of a nonbiological ATP binding protein for improved folding stability. *Chem. Biol 11*, 865–874.

(15) Mansy, S. S., Zhang, J. L., Kummerle, R., Nilsson, M., Chou, J. J., Szostak, J. W., and Chaput, J. C. (2007) Structure and evolutionary analysis of a non-biological ATP-binding protein. *J. Mol. Biol. 371*, 501–513.

(16) Smith, M. D., Rosenow, M. A., Wang, M., Allen, J. P., Szostak, J. W., and Chaput, J. C. (2007) Structural insights into the evolution of a non-biological protein: importance of surface residues in protein fold optimization. *PLoS ONE 2*, e467.

(17) Simmons, C. R., Stomel, J. M., McConnell, M. D., Smith, D. A., Watkins, J. L., Allen, J. P., and Chaput, J. C. (2009) A synthetic protein selected for ligand binding affinity mediates ATP hydrolysis. *ACS Chem. Biol. 4*, 649–658.

(18) Simmons, C. R., Magee, C. L., Smith, D. A., Lauman, L., Chaput, J. C., and Allen, J. P. (2010) Three-dimensional structures reveal multiple ATP/ADP binding modes for a synthetic class of artificial proteins. *Biochemistry 49*, 8689–8699.

(19) Holm, L., and Sander, C. (1996) Mapping the protein universe. *Science 273*, 595–602.

(20) Keep, N. H., Ward, J. M., Robertson, G., Cohen-Gonsaud, M., and Henderson, B. (2006) Bacterial resuscitation factors: revival of viable but non-culturable bacteria. *Cell. Mol. Life Sci. 63*, 2555–2559.

(21) Oliver, J. D. (2010) Recent findings on the viable but nonculturable state in pathogenic bacteria. *FEMS Microbiol. Rev 34*, 415–425.

(22) Walsh, C. (2003) Where will new antibiotics come from? *Nat. Rev. Microbiol. 1*, 65–70.

(23) Krause, M., Rosch, P., Radt, B., and Popp, J. (2008) Localizing and identifying living bacteria in an abiotic environment by a combination of raman and fluorescence microscopy. *Anal. Chem. 80*, 8568–8575.

(24) Rabinowitz, J. D., and White, E. (2010) Autophagy and metabolism. *Science 330*, 1344–1348.

(25) Greenspan, P., Mayer, E. P., and Fowler, S. D. (1985) Nile Red: a selective fluerescent stain for intracellular lipid droplets. *J. Cell Biol. 100*, 965–973.

(26) Doetsch, R. N. (1981) Determinitve methods of light microscopy, in *Manual of Methods for General Bacteriology* (Gerhardt, P., Murray, R. G. E., Costilow, R. N., Nester, E. W., Wood, W. A., Krieg, N. R., and Phillips, G. B., Ed.), pp 21–33, American Society of Microbiology, Washington, DC.

(27) Oliver, J. D. (2005) The viable but nonculturable state in bacteria. *J. Microbiol 43*, 93–100.

(28) Torres-Cabassa, A. S., and Gottesman, S. (1986) Capsule synthesis in *Escherichia coli* K-12 is regulated by proteolysis. *J. Bacteriol. 169*, 981–989.

(29) Trisler, P., and Gottesman, S. (1984) lon transcriptional regulation of genes necessary for capsular polysaccharide synthesis in Escherichia coli K-12. *J. Bacteriol. 160*, 184–191.

(30) Rawls, R. (2000) "Synthetic biology" makes its debut. *Chem. Eng. News*, 49–53.

(31) Phillips, P. C. (2008) Epistasis - the essential role of gene interactions in the structure and evolution of genetic systems. *Nat. Rev. Genet. 9*, 855–867.

(32) Wagner, G. P., Kenney-Hunt, J. P., Pavlicev, M., Peck, J. R., Waxman, D., and Cheverud, J. M. (2008) Pleiotropic scaling of gene effects and the 'cost of complexity'. *Nature 452*, 470–472.

(33) Harry, E., Monahan, L., and Thompson, L. (2006) Bacterial cell division: the mechanism and its precision. *Int. Rev. Cytol. 253*, 27–94.

(34) Chen, G. Z., and Schellhorn, H. E. (2003) Controlled induction of the RpoS regulon in Escherichia coli using an RpoS-expressing plasmid. *Can. J. Microbiol. 49*, 733–740.

(35) Suefuji, K., Valluzzi, R., and RayChaudhuri, D. (2002) Dynamic assembly of MinD into filament bundles modulated by ATP, phospholipids, and MinE. *Proc. Natl. Acad. Sci. U.S.A. 99*, 16776–16781.

(36) Yim, L., Vandenbussche, G., Mingorance, J., Rueda, S., Casanova, M., Ruysschaert, J. M., and Vicente, M. (2000) Role of the carboxy terminus of Eschericia coli FtsA in self-interaction and cell division. *J. Bacteriol. 182*, 6366−6373.
(37) Benner, S. A. (2004) Redesigning genetics. *Science 306*, 625−626.
(38) Johnson, M. S., and Taylor, B. L. (1993) Comparison of methods for specific depletion of ATP in Salmonella typhimurium. *Appl. Environ. Microbiol. 59*, 3509−3512.
(39) Farese, R. V., and Walther, T. C. (2009) Lipid droplets finally get a little R-E-S-P-E-C-T. *Cell 139*, 855−860.
(40) Markham, P. (1994) Occlusions of septal pores in filamentous fungi. *Mycol. Res. 98*, 1089−1106.
(41) van Driel, K. G. A., van Peer, A. F., Grijpstra, J., Wosten, H. A. B., Verkleij, A. J., Muller, W. H., and Boekhout, T. (2008) Septal pore cap protein SPC18, isolated from the basidiomycetous fungus Rhizoctonia solani, also resides in pore plugs. *Eukaryot. Cell 7*, 1865−1873.
(42) Rovner, S. L. (2009) Bacteria boast unexpected order. *Chem. Eng. News*, 42−45.
(43) Xu, H. S., Roberts, N., Singleton, F. L., Attwell, R. W., Grimes, D. J., and Colwell, R. R. (1982) Survival and viability of nonculturable Escherichia coli and Vibrio cholerae in the estuarine and marine environment. *Microb. Ecol. 8*, 313−323.
(44) Hayes, C. S., and Low, D. A. (2009) Signals of growth regulation in bacteria. *Curr. Opin. Microbiol. 12*, 667−673.
(45) Lu, T. K., and Collins, J. J. (2007) Dispersing biofilms with engineered enzymatic bacteriophage. *Proc. Natl. Acad. Sci. U.S.A. 104*, 11197−11202.
(46) Lu, T. K., and Collins, J. J. (2009) Engineered bacteriophage targeting gene networks as adjuvants for antibiotic therapy. *Proc. Natl. Acad. Sci. U.S.A. 106*, 4629−4634.
(47) Waldo, G. S., Standish, B. M., Berendzen, J., and Terwilliger, T. (1999) Rapid protein-folding assay using green fluorescence protein. *Nat. Biotechnol. 17*, 691−695.
(48) Schmidt, M. B. (1990) A locus affecting nucleoid segregation in Salmonella typhimurium. *J. Bacteriol. 172*, 5416−5424.
(49) He, B., Liu, X., Yue, W., Zhou, A., Luo, J., and Cai, X. (2009) Rapid detection of bacteria without cultivation with a portable bioluminescence sensor system. *Afr. J. Microbiol. Res. 3*, 575−580.